Radiosynthesis and Preliminary Biological Evaluation of [^{18}F]VC701, a Radioligand for Translocator Protein

Giuseppe Di Grigoli, Cristina Monterisi,* Sara Belloli, Valeria Masiello, Letterio Salvatore Politi, Salvatore Valenti, Marco Paolino, Maurizio Anzini, Mario Matarrese, Andrea Cappelli, and Rosa Maria Moresco*

Abstract

Positron emission tomography (PET) can be used to monitor in vivo translocator protein (TSPO) expression by using specific radioligands. Recently, several [^{11}C]PK11195 analogues have been synthesized to improve binding stability and brain availability. [^{18}F]VC701 was synthesized and validated in CD healthy rats by biodistribution and inhibition analysis. Imaging studies were also conducted on animals injected unilaterally in the striatum with quinolinic acid (QA) to evaluate the TSPO ligand uptake in a neuroinflammation/neurodegenerative model. [^{18}F]VC701 was synthesized with a good chemical and radiochemical purity and specific activity higher than 37 GBq/μmol. Kinetic studies performed on healthy animals showed the highest tracer biodistribution in TSPO-rich organs, and preadministration of cold PK11195 caused an overall radioactivity reduction. Metabolism studies showed the absence of radiometabolites in the rat brain of QA lesioned rats, and biodistribution analysis revealed a progressive increase in radioactivity ratios (lesioned to nonlesioned striatum) during time, reaching an approximate value of 5 4 hours after tracer injection. These results encourage further evaluation of this TSPO radioligand in other models of central and peripheral diseases.

T*HE TRANSLOCATOR PROTEIN (TSPO)* is a transmembrane multimeric protein complex mainly located in the outer mitochondrial membrane of cells.[1] The physiologic role of TSPO is mostly related with steroidogenesis, but its involvement in the regulation of apoptosis, proliferation, differentiation, and, more recently, mitochondria-related cell death makes it a potential novel target for therapy.[2,3]

Under physiologic conditions, TSPO is present at high concentration in peripheral organs such as kidney, lung, heart, spleen, and adrenals, whereas lower levels are detectable in brain parenchyma.[4] However, thanks to its overexpression on activated macrophages and microglia, TSPO has been widely used for the in vivo imaging of immune system activation in different brain disorders.[5–7] The interest in TSPO ligands also included inflammatory diseases in peripheral regions, tumors, and recently, myocardial dysfunction.[8–11]

[^{11}C]PK11195 was the first nonbenzodiazepine ligand found to bind the TSPO with nanomolar affinity[12] but, despite the large numbers of findings resulting from its use, it is characterized by a low signal to noise ratio and short half-life limitations.[13,14] Recently, several fluorine-18 TSPO radiopharmaceuticals, belonging to several chemical classes, displayed a favorable biological and kinetic profile for in vivo studies. In particular [^{18}F]FEDAA1106,[15] [^{18}F]DPA-714,[16,17] [^{18}F]PBR06,[18] [^{18}F]FEPPA,[19] and [^{18}F]PBR111[20] have been extensively evaluated in animal models of diseases, and some of them are currently under clinical development.

Recent findings showed that the human single nucleotide (HSN) polymorphism rs6971 in exon 4 of the TSPO gene influences the binding profile of most of the radioligands indicated above, allowing us to distinguish in vitro and in vivo populations of high-, low-, and mixed-affinity binding sites.[21–23] Conversely, [^{11}C]PK11195 displays the same binding capacity independently from the isoform expressed, and, recently, new compounds of the same family of [^{11}C]PK11195 but with a higher affinity for the target and lower lipophilicity have been developed showing low sensitivity for the HSN polymorphism rs6971.[24]

* *Authors who contributed equally to this work.*

From IBFM-CNR, Segrate, Italy; Experimental Imaging Center, Division of Nuclear Medicine, and Neuroradiology Department and Neuroradiology Research Group, IRCCS San Raffaele Scientific Institute, Milan, Italy; Department of Health Sciences, University of Milan-Bicocca, Monza, Italy; and Department of Biotechnology, Chemistry and Pharmacy, University of Siena, Siena, Italy.

Address reprint requests to: Prof. Rosa Maria Moresco, University of Milan-Bicocca, Via Fratelli Cervi 93, 20090, Segrate (MI), Italy; e-mail: moresco.rosamaria@hsr.it.

DECKER

In a previous work, we synthesized a series of 3-halomethyl-2-quinolinecarboxamide TSPO ligands structurally related to PK11195. Among them, the most potent compound, the fluoromethyl derivative VC701 showing a half-maximal inhibitory concentration value of 0.11 nM, was labeled by N-[11C]methylation.[25] Encouraged by the favorable in vivo kinetic profile of the tracer, in this article, we describe the labeling of VC701 with fluorine 18. The biological and kinetic profile of [18F]VC701 has been validated in healthy rats and in the quinolinic acid (QA) model of neuroinflammation/neurodegeneration, previously used by our facility to compare other TSPO ligands to [11C]PK11195.[13]

Materials and Methods

Chemicals

All chemicals were of reagent grade. Synthesis procedures are described elsewhere.[25] The precursor VC622 was prepared as described elsewhere, whereas the cold standard VC701 (Figure 1) was synthesized by means of a nucleophilic substitution of the chlorine atom of the precursor with fluoride in the presence of 18-crown-6.[25,26] Reagents and solvents were obtained from Sigma-Aldrich Italia S.p.A (Milan, Italy) and from ABX (Radeberg, Germany) and were high-performance liquid chromatography (HPLC) or American Chemical Society (ACS) grade.

Radiochemistry

The radiosynthesis process was performed with the automated synthesizer TRACERLAB$_{FX-FN}$ (GE Healthcare, Milan Italy). [18F]F$^-$ was produced with the $^{18}O(p,n)^{18}F$ nuclear reaction by irradiation of [18O]water (> 98% atom) using an 18 MeV (Cyclone IBA 18/9, Ottignies-Louvain-La-Neuve, Belgium) or 11 MeV (Siemens CTI, Munich, Germany) cyclotron. Fluorine 18 was separated from $H_2^{18}O$ using a preactivated anion exchange cartridge (QMA Cartridge, ABX). Enriched water was recovered in a vial, whereas [18F]F$^-$ retained on the cartridge was eluted and flushed into the

reactor using a mixture of the crown ether Kryptofix 2.2.2 and K_2CO_3. After an anhydrification step under vacuum and helium at 60°C for 5 minutes and then at 120°C for an additional 5 minutes, the labeling was performed with the precursor VC622 in anhydrous dimethyl sulfoxide (DMSO; Sigma-Aldrich) at 140°C for 20 minutes. After dilution with mobile phase (CH$_3$CN/sodium dihydrogen orthophosphate 1-hydrate 0.05 M, 60/40 (v/v)), the reaction mixture was injected in a semipreparative Sykam HPLC Pump model S1021 for the purification of the compound from other impurities. The fraction of [18F]VC701 was collected in sterile water and recovered by solid-phase extraction on a Sep-Pak tC-18 cartridge. [18F]VC701 was recovered with ethanol and saline solution for the final formulation.

The purification by semipreparative HPLC was performed with an ACE C18 column (5 μm, 250 × 10 mm, CPS, Milan, Italy) using a (Sykam, Fürstenfeldbruck, Germany) HPLC Pump and monitoring with an ultraviolet (UV) detector K-2001 (Knauer, Berlin, Germany) set at 254 nm, in series with a radiochemical detector (Centronic, Wartenberg, Germany) using a mobile phase of CH$_3$CN/sodium dihydrogen orthophosphate 1-hydrate 0.05 M, 60/40 (v/v) at a 4 mL/min flow rate. Retention times were 12 and 19 minutes for precursor and [18F]VC701, respectively.

The quality control was performed on a reversed-phase HPLC analytical column (ACE C18, 5 μm, 250 × 4.6 mm, CPS) using a chromatographic system equipped with a Waters 1515 isocratic pump, a variable-wavelength UV detector (Waters 2487, Milan, Italy) in series with a radiochemical detector (β$^+$-Bioscan Flow Count, WA, USA), using a mobile phase of CH$_3$CN/sodium dihydrogen orthophosphate 1-hydrate 0.025 M, 75/25 (v/v) at 254 nm and a 1 mL/min flow rate. Retention time was about 7 minutes for [18F]VC701.

Data collection and HPLC control were performed with the use of the chromatography software *Empower* 2 (Waters Corporation, Milford, MA).

Mass Characterization of [18F]VC701

For mass characterization, [18F]VC701 was recovered by elution with ethanol. The peak was collected in the sterile vial and its identity confirmed by mass spectrometry (MS). For the analysis, an API QStar Pulsar instrument (Applied BioSystem) was used, with an offline nanospray ESI-MS (Electrospray Ionization-Mass Spectrometry, Applied biosystems, Waltham, MA) ionization source and a time of flight quadrupole analyzer. The mass spectra displayed a relatively short peak at m/z 385 corresponding to the protonated molecular ion (MH$^+$), which confirms the presence of our
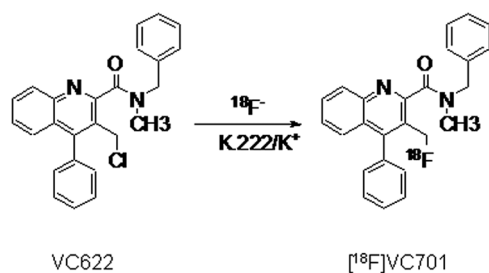
Figure 1. Radiosynthesis scheme of [18F]VC701.

compound. The MS/MS spectrum showed an intense peak at m/z 365 corresponding to the loss of hydrofluoric acid during fragmentation of the parent ion and a very intense peak at m/z 91, which refers to the tropylium ion resulting from the benzylic scission.

Preclinical Evaluation

The kinetics and pharmacologic properties of [18F]VC701 were evaluated in healthy animals. Metabolic analysis and regional distribution were further evaluated in the unilateral striatal QA model at different times after neurotoxin administration. To study the possible involvement of blood-brain barrier (BBB) disruption, in vivo positron emission tomography (PET) studies were paralleled with gadolinium (Gd)-enhanced magnetic resonance imaging (MRI) acquisitions.

Animals

Male CD rats (200–250 g, Charles River, Italy) were used for this study. All the procedures involving the animals and their care were conducted in conformity with the relative institutional guidelines, which comply with relevant national (no. 116, G.U., suppl. 40, 18/2/1992, no. 8, G.U., 14/7/1994) and international laws and policies (EEC Council Directive 86/609, OJ L 358,1, December 12, 1987). The animals were handled and kept in compliance with the Ethics Committee regulations on the care and use of experimental animals (Institutional Animal Care and Use Committee) of San Raffaele Hospital (Milan, Italy).

Biodistribution and Competition Studies in Healthy Animals

CD rats were injected in the tail vein with 2.76 ± 0.47 MBq of [18F]VC701. At 10, 30, 60, 120, and 240 minutes, rats (n = 3 for each time point) were sacrificed and blood was collected into a heparinized tube. Plasma was separated by centrifugation, and 100 μL of blood and plasma was counted in a gamma counter (LKB Compugamma CS 1282). Immediately after sacrifice, cerebellum, cortex, heart, lung, liver, kidney, adrenal gland, spleen, intestine, muscle, spinal cord, and bone were sampled and washed with cold saline. Tissues were placed in preweighed tubes and counted. Radioactivity concentration was calculated as a percentage of the injected dose per gram of tissue (% ID/g tissue).

Competition studies were performed 60 minutes after tracer administration (n = 5 per group), injecting intraperitoneal cold PK11195 (5 mg/kg in vehicle: saline with 5% EtOH and 5% DMSO) or vehicle 1 minute prior to intravenous injection of 3.64 ± 0.11 MBq of [18F]VC701. Statistical analysis was performed using the Student t-test.

Unilateral Intrastriatal QA Animal Model

Unilateral striatal injection with QA was performed as previously described.[27] Briefly, QA solution (0.7 μL of 300 nM/μL; Sigma-Aldrich, Italy) and phosphate-buffered saline (PBS; 0.1 M, 0.7 μL; Euroclone, Italy) were administered in the right and left striata, respectively, according to the stereotaxic coordinates for the target sites (anterior posterior = +0.5, lateral = ±2.6, ventral = −6.5 mm).

Metabolite Analysis

Seven days after QA surgery, animals (n = 3) were injected with 16.5 ± 1.1 MBq of [18F]VC701 in the tail vein and sacrificed 60 minutes later. Blood, nonlesioned brain regions, and lesioned striata were collected and processed for the analysis. Aliquots of 500 μL of plasma were extracted with CH_3CN (1:1 v/v) and filtered. Brain samples were homogenized in saline (saline 1:1 v/v) and processed as described for plasma. Plasma and brain extracts were injected in HPLC (Gilson, USA). Analyses were performed at room temperature (column XTerra RP18, 300 × 7.8 mm, 10 μM) with CH_3CN/phosphoric acid (0.05 M 60/40, v/v) as mobile phase at the flow rate of 5 mL/min. Eluted fractions were collected every 30 seconds for 14 minutes and counted with a gamma counter to obtain counts per minute (cpm).

Ex Vivo Cerebral Biodistribution Studies

Tissue sampling Analysis was performed 7 days after QA injection, animals (n = 3 per group) were injected in the tail vein with 5.5 ± 1.5 MBq of [18F]VC701 and sacrificed by decapitation after 60, 120, and 240 minutes. Lesioned and nonlesioned striata, right and left cortex, and cerebellum were processed as described above. Statistical analysis was performed using the Student t-test.

Autoradiography For autoradiography studies, animals (n = 3 per group) at 7, 40, and 60 days after QA administration were injected in the tail vein with 7.5 ± 1.2 MBq of [18F] VC701 and sacrificed 60 minutes later. Brains were rapidly removed, placed in the Brain Matrix (Stoelting Co, USA), and cut into 2 mm slice coronal sections that were exposed to phosphor screen for 3 hours and developed with PhosphorImager (Perkin Elmer, Italy). Images were visualized using OptiQuant (PerkinElmer) and ImageJ 1.37v (Wayne Rasband, National Institutes of Health, Bethesda, MD) software. Radioactivity concentrations were calculated using region of interest (ROI) analysis. A circular ROI (15 mm^2) was manually drawn in the region of maximum uptake of the striatum in the lesioned side and then symmetrically

copy-pasted in contralateral striatum, used as the TSPO-free reference region. Radioactivity concentration was calculated as a percentage of the injected dose per square millimeter of tissue (% ID/mm^2). Target to background ratio (TBR) was defined as the ratio between the radioactivity concentration in the lesioned striatum versus the nonlesioned striatum. Statistical analysis was performed using the Student *t*-test.

In Vivo Longitudinal Imaging Studies

A separate group of animals (*n* = 3) was monitored in vivo with both PET and MRI at three different time points after QA administration.

The intracerebral distribution of [^{18}F]VC701 was evaluated with PET at 7, 40, and 60 days after QA as follows: animals were anesthetized with 2% isoflurane in air, positioned prone on the PET (YAP-S-PET II, ISE, Italy) scanner bed with the brain centered in the field of view, and injected in the tail vein with 5.5 ± 0.7 MBq of [^{18}F]VC701. Acquisition started 100 minutes after radiotracer injection and lasted 50 minutes.

MRI was performed on the same animals the day after PET acquisition using a 3 T human-grade MRI scanner and a rat-dedicated volumetric coil of 40 mm diameter (Philips Medical Systems, the Netherlands) as follows: rats were anesthetized (intraperitoneally) with tribromoethanol 1.7% solution (20 μL/g of rat weight), and 0.3 mmol/kg of gadobutrolo (Gadovist, Bayer) was injected in the tail vein. The animal was positioned prone on the MRI bed, and a spin echo T$_1$-weighted sequence was acquired on the coronal plane.

PET images were coregistered with MRI and analyzed with *PMOD* 3.2 v (PMOD Technologies Ltd, Switzerland). The [^{18}F]VC701 radioactivity concentrations were calculated using ROI analysis. A circular ROI (17 mm^2) was manually drawn in the core of the striatal lesion on the MRI and then copied on the coregistered PET images on three consecutive transaxial slices. ROI were then symmetrically pasted into the contralateral striatum used as a reference region. Radioactivity concentration was calculated as a percentage of the injected dose per gram of tissue (% ID/g). As for autoradiography studies, TBR was defined as the ratio between radioactivity concentration in the lesioned striatum versus the nonlesioned striatum. Statistical analysis was performed using the Student *t*-test.

Results

Radiosynthesis

Radiosynthesis, including ^{18}F-fluorination, HPLC purification, and radiopharmaceutical formulation, was completed

in about 80 minutes from the end of bombardment with a 10 to 15% radiochemical yield (not decay corrected), a chemical and radiochemical purity > 95%, and a specific activity > 37 GBq/μmol at the end of the synthesis. In a typical experiment, starting from 18.5 to 22.5 GBq of [^{18}F]F$^-$, 2.9 to 3.7 GBq of [^{18}F]VC701 was obtained (see Figure 1).

The identity of the final radiotracer was confirmed by the coinjection of [^{18}F]VC701 with its cold standard on HPLC and by MS analysis.

Preclinical Evaluation

Biodistribution and Inhibition Studies in Healthy Animals

[^{18}F]VC701 was progressively taken up and retained in tissues rich in TSPO, such as heart, adrenal gland, spleen, lungs, and kidney (Table 1). In these organs, radioactivity concentration reached maximum values after 1 hour (approximately 4 %ID/g) and slowly decreased thereafter. At 240 minutes after injection, radioactivity concentration was still higher than 2 %ID/g, except for kidneys. The slow rate of washout from target organs promoted a progressive increase in target tissue to plasma (T/P) ratios with maximum values at 120 minutes postinjection. Intermediate values of radioactivity were also observed in the intestine, whereas in the remaining tissues, including bone and spine, the uptake was < 1 %ID/g or negligible. Brain uptake was definitely lower than that observed in the periphery even if penetration was high, as indicated by T/P ratios (cerebral cortex/plasma; 60 minutes: T/P = 8.0; 120 minutes: T/P = 7.0). However, in agreement with regional TSPO expression, radioactivity concentration in cerebellum was higher than that measured in the whole cortex. Finally, due to the presence of TSPO in blood cells, we found whole blood to plasma ratios reaching maximum values of 6 at 1 hour after injection.

The specificity of tracer uptake in various organs was confirmed by competition experiments with PK11195 (see Table 1). In all tissues examined, with the exclusion of adrenal glands, preadministration of 5 mg/kg of PK11195 significantly reduced (*p* < .05, Student *t*-test) the tracer uptake. The percentage of reduction ranged from a minimum of 37% for the liver to a maximum of 88% for the lungs. In agreement with what was previously described for the majority of TSPO ligands, in the adrenal glands, we observed only a partial and not significant inhibition of radioactivity uptake.

Metabolite Analysis

Sixty minutes after [^{18}F]VC701 administration, plasma samples showed the presence of two radioactive metabolites

Table 1. [^{18}F]VC701 Biodistribution Values in Healthy Animals

Tissue	%ID/g	At 10 min (n = 3)	At 30 min (n = 3)	At 60 min (n = 5) Vehicle	At 60 min (n = 5) PK11195	At 120 min (n = 3)	At 240 min (n = 3)
Blood		0.31 ± 0.04	0.11 ± 0.01	0.12 ± 0.01	0.04 ± 0.00*	0.06 ± 0.03	0.04 ± 0.01
Plasma		0.12 ± 0.11	0.03 ± 0.01	0.02 ± 0.00	0.03 ± 0.01	0.01 ± 0.00	0.01 ± 0.00
Heart		0.61 ± 0.09	1.23 ± 0.23	3.90 ± 0.79	1.00 ± 0.20*	2.28 ± 0.75	2.02 ± 0.07
Lung		2.14 ± 0.66	2.57 ± 0.62	5.50 ± 2.10	0.71 ± 0.30*	2.37 ± 0.66	2.29 ± 0.29
Kidney		0.45 ± 0.04	1.04 ± 0.22	2.33 ± 0.40	0.72 ± 0.20*	1.44 ± 0.46	1.35 ± 0.23
Liver		0.28 ± 0.02	0.48 ± 0.13	0.58 ± 0.10	0.41 ± 0.11*	0.32 ± 0.17	0.37 ± 0.16
Spleen		0.46 ± 0.28	1.68 ± 0.45	3.78 ± 0.23	0.91 ± 0.41*	2.56 ± 0.92	2.43 ± 0.24
Adrenal glands		0.39 ± 0.08	1.63 ± 0.60	4.01 ± 1.67	2.61 ± 1.10	2.52 ± 0.41	2.79 ± 1.21
Bone		0.08 ± 0.01	0.24 ± 0.05	0.56 ± 0.11	0.34 ± 0.07*	0.50 ± 0.05	0.53 ± 0.05
Intestine		0.07 ± 0.03	0.56 ± 0.37	1.82 ± 0.37	0.64 ± 0.43*	1.47 ± 0.77	0.77 ± 0.11
Muscle		0.03 ± 0.00	0.09 ± 0.02	0.43 ± 0.12	0.09 ± 0.04*	0.12 ± 0.11	0.12 ± 0.01
Spine		0.08 ± 0.00	0.19 ± 0.01	0.47 ± 0.06	0.20 ± 0.06*	0.34 ± 0.04	0.37 ± 0.05
Cerebral cortex		0.12 ± 0.00	0.12 ± 0.02	0.16 ± 0.01	0.04 ± 0.01*	0.07 ± 0.01	0.05 ± 0.02
Cerebellum		0.12 ± 0.01	0.14 ± 0.02	0.20 ± 0.02	0.04 ± 0.01*	0.10 ± 0.00	0.06 ± 0.04

Radioactivity concentration is expressed as a percentage of injected dose per gram of tissue (%ID/g). Values are expressed as mean ± SD. PK11195 dose: 5 mg/kg. Vehicle: saline with 5% EtOH and 5% DMSO.
*$p < .05$ versus 60-minute vehicle, Student t-test.

more polar than the parent compound (retention times: 2 and 3 minutes; parent compound: 8.5 minutes) that accounted for 30 ± 0.9% and 8.9 ± 2.1% of total radioactivity in plasma. On the contrary, in both QA-injected lesioned striatum and nonlesioned extrastriatal regions, no radiometabolites were observed, and the fraction of parent compound accounted for more than 99% of radioactivity, indicating that brain signal is uniquely given by unmetabolized radiotracer.

Ex Vivo Cerebral Biodistribution Studies

Tissue sampling In tissue sampling studies performed at 7 days after QA administration, we observed that radioactivity uptake in the lesioned side of the brain was maximum at 60 minutes postinjection and remained stable thereafter (120 and 240 minutes). On the contrary, in nonlesioned striatum, radioactivity concentration was progressively cleared. [^{18}F]VC701 uptake measured in

**Table 2.** Ex Vivo [^{18}F]VC701 Biodistribution and Autoradiography Values in QA Animals

Ex Vivo Tissue Sampling		7 days		
		60 min	120 min	240 min
Tissue	UM	(n = 3)	(n = 3)	(n = 3)
Striatum QA	%ID/g	0.20 ± 0.05*	0.08 ± 0.02*	0.068 ± 0.05*
Striatum PBS	%ID/g	0.09 ± 0.02	0.03 ± 0.01**	0.013 ± 0.001
Striatum QA/striatum PBS	%ID/g/%ID/g	2.10 ± 0.17	2.66 ± 0.19	5.23 ± 1.25
Striatum QA/plasma	%ID/g/%ID/g	8.41 ± 1.72	13.3 ± 0.95	24.6 ± 5.90
Ex Vivo Autoradiography	UM	7 days	40 days	60 days
		60 min	60 min	60 min
Tissue/Tissue		(n = 3)	(n = 3)	(n = 3)
Striatum QA/striatum PBS	%ID/mm^2/%ID/mm^2	2.03 ± 0.5	1.44 ± 0.24	1.67 ± 0.04

PBS = phosphate-buffered saline; QA = quinolinic acid; UM = unit of measurement.
Radioactivity concentration is expressed as a percentage of injected dose per gram/per square area of brain tissue (%ID/g or %ID/mm^2). Values are expressed as mean ± SD.
*$p < .05$ versus striatum PBS.
**$p < .05$ versus striatum PBS at 240 minutes, Student t-test.
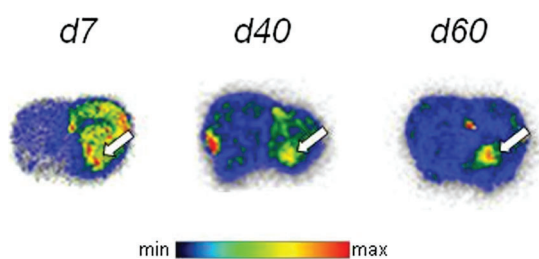
Figure 2. Autoradiography images obtained 7, 40, and 60 days after quinolinic acid injury, 60 minutes after [18F]VC701 injection. *Arrows* indicate maximum [18F]VC701 uptake in injured striatal regions. Radioactivity spot in the left nonlesioned side indicates the presence of cerebral vessels.

lesioned striatum was significantly higher than that observed in nonlesioned striatum independently from the time of the analysis (Table 2).

Autoradiography Similar results were obtained with autoradiography showing an increase in [18F]VC701 uptake in the lesioned region 7 days after injury compared to the contralateral side. In addition, autoradiography studies revealed that areas of increased radioactivity distribution were still present at 60 days after QA administration, also involving ipsilateral cortical regions, particularly at early times postinjury (Figure 2). The ROI analysis showed a TBR of 2.03, 1.44, and 1.67, respectively, at 7, 40, and 60 days postinjury (Table 2).

In Vivo Longitudinal Imaging Studies

PET [18F]VC701 studies enabled the visualization of increased radioactivity concentration in lesioned brain areas, with a pattern of distribution similar to that observed using autoradiography (Figure 3A). Longitudinal evaluation performed on the same animals revealed a maximum value of lesioned to nonlesioned ratio at 7 days postinjury (radioactivity concentrations: 0.055 ± 0.005 %ID/g and $0.040 \pm$
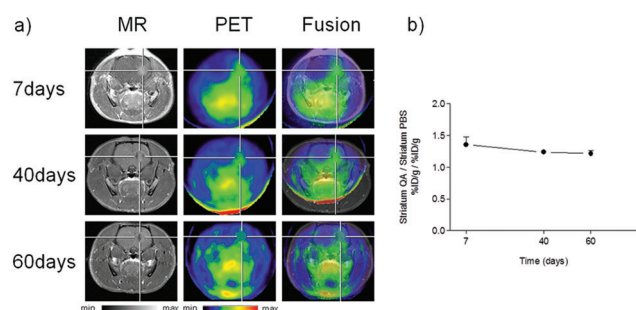
Figure 3. a) *Left column:* Post-Gd T_1 MRIs. *Middle column:* Transaxial PET images. *Right column:* [18F]VC701 PET images merged with MRI. b) Striatum quinolinic acid (QA)/striatum phosphate-buffered saline (PBS) ratio obtained 7, 40, and 60 days postinjury using region of interest analysis.

0.004 %ID/g, $p < .05$ in lesioned and nonlesioned striatum, respectively; TBR: 1.37). As observed with autoradiography, lesions were also present in extrastriatal areas and were still present at 40 and 60 days, although TBR values decreased to 1.23 and 1.21 at 40 and 60 days, respectively (Figure 3B).

Contrast-enhanced T_1-weighted MRIs showed BBB leakage and Gd enhancement in the right striatum 8 days postinjury. A brain malacic lesion with neural loss, but not contrast enhancement, was visible in the right striatum about 40 and 60 days after QA administration.

Discussion

The aim of this work was to develop a structural analogue of [11C]PK11195 labeled with [18F]fluorine. We previously demonstrated a favorable biological profile of the compound VC701 developed by Cappelli and colleagues and labeled with carbon 11[25,26] for the in vivo visualization of TSPO.[13] The radioligand [18F]VC701 was efficiently synthesized by nucleophilic substitution of the chlorine atom with NCA 18F-fluoride ion, with good radiochemical yield and specific activity.

Ex vivo studies in healthy rats showed a significant increase in [18F]VC701 distribution in tissues rich in TSPO, with maximum uptake achieved 60 minutes after tracer administration. Peripheral distributions were comparable to those observed for other TSPO ligands, belonging to different chemical classes, with higher accumulation in heart, lungs, spleen, and adrenals.[16,28–30] Tracer uptake specificity was confirmed by competition experiments in healthy rats: in organ expressing TSPO, PK11195 injection produced a significant reduction in radioactivity concentration that ranged from 87% (lungs) to 34% (adrenal glands). In contrast to other fluorinated TSPO radioligands, we observed low accumulation of radioactivity in bone, indicating negligible levels of defluorination.[28]

[18F]VC701 represented in plasma the 61% of total radioactivity, whereas no radiometabolites were observed in the brain, confirming that the signal detected was exclusively due to the parent compound. Metabolic stability was similar to that reported for other fluorinated tracers[31–33] but better than [11C]PK11195, where 10% of brain radioactivity is due to radiometabolites.[34]

The biodistribution of [18F]VC701, measured by tissue sampling at 1 week after QA injection, reached its maximum value 60 minutes after tracer administration and remained stable thereafter. On the contrary, a progressive clearance of radioactivity was observed in normal brain tissue. This caused a time-dependent increase in TBRs that reached an approximate value of 5 4 hours after tracer injection.

With the obvious limits of a lack of a direct comparison, signal to background ratios observed with [^{18}F]VC701 were definitely higher than those previously obtained by our group with [^{11}C]PK11195 in the same animal model.[13,27] A direct comparison with the other radioligands used in this animal model is challenging because of differences in QA protocols (doses, stereotaxic coordinates, etc.); however, similar or higher ratios were described in not overlapping QA model by James and colleagues using [^{18}F]DPA714[16] and by Arlicot and colleagues with [^{125}I]CLINDE.[35]

The high brain penetrability and tissue retention at the target site allowed us to monitor QA-induced lesions in striatal and extrastriatal regions, not only ex vivo with autoradiography, as previously performed using [^{11}C] PK11195,[27] but also in vivo with PET.

In this study, a time window centered at 120 minutes after injection was selected for PET imaging studies. This time frame was chosen because it was a good compromise between radioactivity accumulation at the target site (stable from 60 minutes), washout from normal brain tissue, and study duration. Finally, it must be remembered that the quality of images and absolute quantitative data obtained in vivo by PET strictly depend on the tomograph. Partial volume effect linked to the specific spatial resolution properties of the PET system or the reconstruction algorithm affected image quality and data quantification, thus giving signal to noise ratios lower than those obtained not only using ex vivo techniques but also with the other PET scanner.

Another question concerning the TSPO signal in QA lesioned regions is that it might be influenced by the contribution of BBB integrity. In a recent work in which rats were injected with QA at a low dose (150 nmol), Arlicot and colleagues suggested that TSPO radioligand signal at early times postlesion might also reflect the presence of infiltrating leukocytes migrating from the periphery into lesioned striatum.[35] In this study, we monitored the time course of anatomic disruption of BBB using Gd-enhanced MRI.

T_1-weighted images showed increased Gd uptake in the lesioned striatum at 8 days after QA injection, indicating disruption of BBB, which was restored 40 and 60 days after surgery. No Gd enhancement was present in ipsilateral cortical regions, where we observed an increase in radioactivity. These findings clearly indicated that cortical signal was independent from BBB damage; on the other hand, a partial contribution of peripheral cells migration cannot be excluded at 8 days after surgery. BBB leakage could also influence radioligand delivery; however, it should be noted that uptake difference between the lesioned region and the contralateral side was still present 240 minutes after tracer injection and even detectable 60 days from QA administration when the Gd signal was negligible.

Another debated issue is represented by the contribution of reactive gliosis to TSPO signal.[36] In our precedent study, we demonstrated that the unilateral striatum injection of the neurotoxin caused intense microglia activation, neural loss, and astrocyte gliosis, especially at 8 days postsurgery.[13] Similar results were obtained by Arlicot and colleagues, showing in the QA model intense astrocyte and microglia activation between 7 and 14 days.[35] Consequently, the contribution of astrocytes to [^{18}F]VC701 signal is highly probable, and further immunohistochemical analysis is needed to confirm this statement.

Conclusions

Our results, taken together, showed that the structural analogue of [^{11}C]PK11195, [^{18}F]VC701, is a high-affinity tracer specific for TSPO and potentially useful for the in vivo imaging of neuroinflammation. However, further in vitro studies are required to elucidate the sensitivity of [^{18}F] VC701 for the HSN polymorphism rs6971 of the TSPO gene, also in relation to the recently developed azaisostere analogues of [^{11}C]PK11195.[24]

Acknowledgments

References

1. Papadopoulos V, Baraldi M, Guilarte TR, et al. Translocator protein (18kDa): new nomenclature for the peripheral-type benzodiazepine receptor based on its structure and molecular function. Trends Pharmacol Sci 2006;27:402–9.

2. Caballero B, Veenman L, Gavish M. Role of mitochondrial translocator protein (18 kDa) on mitochondrial-related cell death processes. Recent Pat Endocr Metab Immune Drug Discov 2013;7:86–101.

3. Veenman L, Gavish M. The role of 18 kDa mitochondrial translocator protein (TSPO) in programmed cell death, and effects of steroids on TSPO expression. Curr Mol Med 2012;12: 398–412.

4. Batarseh A, Papadopoulos V. Regulation of translocator protein 18 kDa (TSPO) expression in health and disease states. Mol Cell Endocrinol 2010;327:1–12.

5. Harberts E, Datta D, Chen S, et al. Translocator protein 18 kDa (TSPO) expression in multiple sclerosis patients. J Neuroimmune Pharmacol 2013;8:51–7.

6. Politis M, Pavese N, Tai YF, et al. Microglial activation in regions related to cognitive function predicts disease onset in Huntington's disease: a multimodal imaging study. Hum Brain Mapp 2011;32:258–70.

7. Iannaccone S, Cerami C, Alessio M, et al. In vivo microglia activation in very early dementia with Lewy bodies, comparison with Parkinson's disease. Parkinsonism Relat Disord 2013;19:47–52.

8. Branley HM, du Bois RM, Wells AU, et al. PET scanning of macrophages in patients with scleroderma fibrosing alveolitis. Nucl Med Biol 2008;35:901–9.

9. Gaemperli O, Shalhoub J, Owen DR, et al. Imaging intraplaque inflammation in carotid atherosclerosis with 11C-PK11195 positron emission tomography/computed tomography. Eur Heart J 2012;33:1902–10.

10. Mukherjee S, Das SK. Translocator protein (TSPO) in breast cancer. Curr Mol Med 2012;12:443–57.

11. Qi X, Xu J, Wang F, et al. Translocator protein (18 kDa): a promising therapeutic target and diagnostic tool for cardiovascular diseases. Oxid Med Cell Longev 2012;2012:162934.

12. Pike VW, Halldin C, Crouzel C, et al. Radioligands for PET studies of central benzodiazepine receptors and PK (peripheral benzodiazepine) binding sites—current status. Nucl Med Biol 1993;20:503–25.

13. Belloli S, Moresco RM, Matarrese M, et al. Evaluation of three quinoline-carboxamide derivatives as potential radioligands for the in vivo pet imaging of neurodegeneration. Neurochem Int 2004;44:433–40.

14. Maeda J, Suhara T, Zhang MR, et al. Novel peripheral benzodiazepine receptor ligand [11C]DAA1106 for PET: an imaging tool for glial cells in the brain. Synapse 2004;52:283–91.

15. Takano A, Piehl F, Hillert J, et al. In vivo TSPO imaging in patients with multiple sclerosis: a brain PET study with [18F]FEDAA1106. EJNMMI Res 2013;3(1):30.

16. James ML, Fulton RR, Vercoullie J, et al. DPA-714, a new translocator protein-specific ligand: synthesis, radiofluorination, and pharmacologic characterization. J Nucl Med 2008;49:814–22.

17. Arlicot N, Vercouillie J, Ribeiro MJ, et al. Initial evaluation in healthy humans of [18F]DPA-714, a potential PET biomarker for neuroinflammation. Nucl Med Biol 2012;39:570–8.

18. Fujimura Y, Zoghbi SS, Simeon FG, et al. Quantification of translocator protein (18 kDa) in the human brain with PET and a novel radioligand, (18)F-PBR06. J Nucl Med 2009;50:1047–53.

19. Rusjan PM, Wilson AA, Bloomfield PM, et al. Quantitation of translocator protein binding in human brain with the novel radioligand [18F]-FEPPA and positron emission tomography. J Cereb Blood Flow Metab 2011;31:1807–16.

20. Kuhnast B, Damont A, Hinnen F, et al. [18F]DPA-714, [18F]PBR111 and [18F]FEDAA1106-selective radioligands for imaging TSPO 18 kDa with PET: automated radiosynthesis on a TRACERLAb FX-FN synthesizer and quality controls. Appl Radiat Isot 2012;70:489–97.

21. Owen DR, Yeo AJ, Gunn RN, et al. An 18-kDa translocator protein (TSPO) polymorphism explains differences in binding affinity of the PET radioligand PBR28. J Cereb Blood Flow Metab 2012;32:1–5.

22. Guo Q, Owen DR, Rabiner EA, et al. Identifying improved TSPO PET imaging probes through biomathematics: the impact of multiple TSPO binding sites in vivo. Neuroimage 2012;60:902–10.

23. Owen DR, Gunn RN, Rabiner EA, et al. Mixed-affinity binding in humans with 18-kDa translocator protein ligands. J Nucl Med 2011;528:24–32.

24. Zanotti-Fregonara P, Zhang Y, Jenko KJ, et al. Synthesis and evaluation of translocator 18 kDa protein (TSPO) positron emission tomography (PET) radioligands with low binding sensitivity to human single nucleotide polymorphism rs6971. ACS Chem Neurosci 2014;5:963–71.

25. Cappelli A, Matarrese M, Moresco RM, et al. Synthesis, labeling, and biological evaluation of halogenated 2-quinolinecarboxamides as potential radioligands for the visualization of peripheral benzodiazepine receptors. Bioorg Med Chem 2006;14:4055–66.

26. Cappelli A, Pericot Mohr G, Gallelli A, et al. Structure-activity relationships in carboxamide derivatives based on the targeted delivery of radionuclides and boron atoms by means of peripheral benzodiazepine receptor ligands. J Med Chem 2003;46:3568–71.

27. Moresco RM, Lavazza T, Belloli S, et al. Quinolinic acid induced neurodegeneration in the striatum: a combined in vivo and in vitro analysis of receptor changes and microglia activation. Eur J Nucl Med Mol Imaging 2008;35:704–15.

28. Zhang MR, Maeda J, Furutsuka K, et al. [18F]FMDAA1106 and [18F]FEDAA1106: two positron-emitter labeled ligands for peripheral benzodiazepine receptor (PBR). Bioorg Med Chem Lett 2003;13:201–4.

29. Fookes CJ, Pham TQ, Mattner F, et al. Synthesis and biological evaluation of substituted [18F]imidazo[1,2-a]pyridines and [18F]pyrazolo[1,5-a]pyrimidines for the study of the peripheral benzodiazepine receptor using positron emission tomography. J Med Chem 2008;51:3700–12.

30. Briard E, Zoghbi SS, Simeon FG, et al. Single-step high-yield radiosynthesis and evaluation of a sensitive 18F-labeled ligand for imaging brain peripheral benzodiazepine receptors with PET. J Med Chem 2009;52:688–99.

31. Chauveau F, Van Camp N, Dolle F, et al. Comparative evaluation of the translocator protein radioligands 11C-DPA-713, 18F-DPA-714, and 11C-PK11195 in a rat model of acute neuroinflammation. J Nucl Med 2009;50:468–76.

32. Van Camp N, Boisgard R, Kuhnast B, et al. In vivo imaging of neuroinflammation: a comparative study between [(18)F]PBR111, [(11)C]CLINME and [(11)C]PK11195 in an acute rodent model. Eur J Nucl Med Mol Imaging 2010;37:962–72.

33. Wadsworth H, Jones PA, Chau WF, et al. [18F]GE-180: a novel fluorine-18 labelled PET tracer for imaging translocator protein 18 kDa (TSPO). Bioorg. Med Chem Lett 2010;22:1308–13.

34. Luoto P, Laitinen I, Suilamo S, et al. Human dosimetry of carbon-11 labeled N-butan-2-yl-1-(2-chlorophenyl)-N-methylisoquinoline-3-carboxamide extrapolated from whole-body distribution kinetics and radiometabolism in rats. Mol Imaging Biol 2010;12:435–42.

35. Arlicot N, Tronel C, Bodard S, et al. Translocator protein (18 kDa) mapping with [125I]-CLINDE in the quinolinic acid rat model of excitotoxicity: a longitudinal comparison with microglial activation, astrogliosis, and neuronal death. Mol Imaging 2014;13:4–11.

36. Lavisse S, Guillermier M, Herard AS, et al. Reactive astrocytes overexpress TSPO and are detected by TSPO positron emission tomography imaging. J Neurosci 2012;32:10809–18.